Photochemistry and Photobiology, 1996, 63(2): 161–168

Phototoxicity of Some Bromine-Substituted Rhodamine Dyes: Synthesis, Photophysical Properties and Application as Photosensitizers

Prabir Pal[1], Hualing Zeng[1], Gilles Durocher*[1], Denis Girard[2], Tiechao Li[2], Ajay K. Gupta[2], Richard Giasson*[2], Louise Blanchard[3], Louis Gaboury*[3], Antonia Balassy[3], Chantal Turmel[3], André Laperrière[3] and Luc Villeneuve*[3]

[1]Laboratoire de photophysique moléculaire and [2]Laboratoire de photochimie organique, Département de chimie, and [3]Laboratoire de pathologie moléculaire, Département de pathologie, Université de Montréal, Montréal, Québec, Canada

Received 6 October 1995; accepted 17 October 1995

ABSTRACT

The synthesis of some bromine-substituted rhodamine derivatives *viz.*, 4,5-dibromorhodamine methyl ester (dye 2) and 4,5-dibromorhodamine *n*-butyl ester (dye 3) are reported. These dyes were synthesized to promote a more efficient cancer cell photosensitizer for potential use in *in vitro* bone marrow purging in preparation for autologous bone marrow transplantation. Spectroscopic and photophysical characterization of these dyes together with rhodamine 123 (dye 1) are reported in water, methanol, ethanol and also in a microheterogeneous system, sodium dodecyl sulfate. The possible mechanism of photosensitization is characterized in terms of singlet oxygen efficiency of these dyes. Singlet oxygen quantum yields for bromine-substituted dyes are in the range of 0.3–0.5 depending on the solvent. For dye 1 no singlet oxygen production is found. The photodynamic actions of these dyes in different cell lines are tested. It was found that dye 2 and dye 3 are efficient photosensitizers and mediate eradication of K562, EM2, myeloid cell lines (CML) and the SMF-AI rhabdomyosarcoma line.

INTRODUCTION

The method for treatment of consolidated single tumors by light-induced sensitization of singlet oxygen was first proposed by Lipson and coworkers (1) and extensively developed by T. Dougherty and collaborators (2–4).

Hematoporphyrin was chosen as a sensitizing dye, and after tumor injection, red light from a laser was introduced to the tumor center *via* a light pipe. Direct spectroscopy showed the effectiveness of dye–singlet oxygen excitation transfer (5). The method has now been approved by the Food and Drug Administration and was introduced in many hospitals. This case represents a remarkable example of technology transfer, from the realms of organic synthesis, pure spectroscopy, quantum chemistry and photochemistry, to a powerful medical advance.

A variety of organic chemicals have been found to be useful as photosensitizers (PS),† where they are initiating specific chemical reactions resulting in therapeutic effects. Among these, as stated above, the use of hematoporphyrin derivatives in photochemotherapy has especially received a great deal of attention. Because *ex vivo* purging, as opposed to *in vivo* photodynamic therapy (PDT), is not submitted to the same stringent requirements for wavelength of absorption and light scattering, one may envisage a whole new range of compounds that may effect cell killing (6–8).

One compound that has recently been shown to exhibit selective distribution in living cells is the laser dye rhodamine 123 (dye **1**). In a series of papers, Chen and co-workers (9, 10) reported that dye **1** is preferentially retained by mitochondria in muscle and carcinoma cells. However, this dye **1** is a relatively weak phototoxin. But because dye **1** has a very high fluorescence quantum yield (ϕ_f = 0.9), a low triplet yield has been reported (11). It has also been reported that dye **1** does not react with molecular oxygen to produce singlet oxygen (12). It is well known that the efficiency of singlet oxygen production by the PS is one of the major factors that govern the extent of photodynamic action. We then made the assumption that singlet oxygen production efficiency might be increased by substitution of a halogen for hydrogen atom in order to increase the intersystem crossing to the triplet state.

We have synthesized two dyes *viz.*, 4,5-dibromorhodamine methyl ester (dye **2**) and 4,5-dibromorhodamine *n*-butyl ester (dye **3**). Singlet oxygen production, the efficiency of crossing the cytoplasmic and mitochondrial membranes and the retention of the dye in mitochondria all govern photodynamic action. For example, hydrophobicity was shown to be an important factor influencing the *in vitro* uptake of porphyrins (13). Different ester forms of rhodamine should have different hydrophobic properties and consequently should affect the extent of photodynamic action.

In this paper we report the synthesis of dye **2** and dye **3**, spectroscopic and photophysical properties of these newly synthesized dyes, together with dye **1** efficiency in PDT.

*Authors to whom correspondence should be addressed at: Dr. Gilles Durocher, Laboratoire de photophysique moléculaire, Département de chimie, Université de Montréal, C. P. 6128, Succ. Centre-ville, Montréal, Québec H3C 3J7, Canada. Fax: 514-343-7586; e-mail: durocher@ere.umontreal.ca.

†*Abbreviations:* MDR, multidrug resistant; PDT, photodynamic therapy; PS, photosensitizer; SDS, sodium dodecyl sulfate; TICT, twisted intramolecular charge transfer.

MATERIALS AND METHODS

Materials

Rhodamine 110 (Eastman Kodak), rhodamine B (Eastman Kodak) and rose bengal (Aldrich) were used without further purification after checking the purity. Rhodamine 123 was purchased from Aldrich and also prepared as described below. Bromine (Aldrich), HCl gas (Liquid Carbonic) and *n*-butanol (Anachemia) were used as received. Dichloromethane (ACP Chemicals) and benzene (BDH) were distilled before use. Spectrophotometric grade solvents were used as received. Double-distilled deionized water was used as solvent. The surfactant, sodium dodecyl sulfate (SDS) (Aldrich, 98%) was used after being purified according to the method reported recently (14). Column chromatographies were carried out using 230–400 mesh silica gel (American Chemicals Ltd).

Rhodamine methyl ester (rhodamine 123) (dye 1). Rhodamine 110 (685.3 mg; 1.87 mmol) was suspended in methanol (75 mL) in a 100 mL three necked round-bottom flask equipped with a condenser and a drying tube containing anhydrous $CaSO_4$. Hydrochloric acid gas was bubbled through the solution for 45 min, during which the solution became homogeneous. The reaction mixture was refluxed 6 h and then stirred overnight at room temperature. The methanol was evaporated under reduced pressure and a dark brown solid residue was obtained. The residue was purified by column chromatography using dichloromethane and increasing concentration of methanol as eluent. Evaporation of fractions containing rhodamine methyl ester (rhodamine 123) afforded a brown residue that was kept under reduced pressure until its weight remained constant. Rhodamine methyl ester (509 mg) was obtained with a 72% yield. The product was used without further purification as starting material in the next step of the synthesis. ^{1}H NMR (300 MHz, CD_3OD): δ 8.32 (dd, J = 1.6 and 7.8 Hz, 1 H, H-6′); 7.82 (m, 2 H, H-4′ and H-5′); 7.45 (dd, J = 1.6 and 7.3 Hz, 1 H, H-3′); 7.02 (d, J = 9.0 Hz, 2 H, H-1 and H-8); 6.82 (d, J = 2.0 Hz, 2H, H-4 and H-5); 6.79, (dd, J = 2.0 and 9.0 Hz, 2H, H-2 and H-7); 3.62 (s, 3 H, CH_3).

4,5-Dibromorhodamine methyl ester (dye 2). Rhodamine methyl ester (rhodamine 123) (509 mg; 1.34 mmol) was dissolved in anhydrous ethanol (50 mL) in a 100 mL round-bottom flask equipped with a condenser. A fresh bromine solution was prepared in a separate vessel by dissolving Br_2 (1.5 mL) in anhydrous ethanol (100 mL). A first portion of this ethanolic bromine solution (9.3 mL; 2.71 mmol of Br_2) was added to the rhodamine 123 solution and the resulting reaction mixture was stirred at room temperature for 71.5 h. The progression of the reaction was monitored by chromatography and two additional portions of fresh bromine solution (2.4 mL; 0.70 mmol of Br_2 and 1.2 mL; 0.35 mmol of Br_2), each followed by 1 h of stirring at room temperature, were necessary to bring the reaction to completion. Evaporation of the reaction mixture under reduced pressure gave a dark brown solid residue. The residue was dissolved in ethanol and evaporated again to dryness five times to make sure that any traces of Br_2 were removed. The residue was pumped under vacuum (0.025 mm Hg) for 13 h at room temperature and for 21 h at 110°C (0.025 mm Hg) in an Abderhalden drying pistol using anhydrous $CaSO_4$ as drying agent. 4,5-Dibromorhodamine methyl ester (dye **2**) was obtained in a quantitative yield (purity >99% by HPLC). ^{1}H RMN (300 MHz, CD_3OD): δ 8.34 (dd, J = 1.7 and 7.5 Hz, 1 H, H-6′); 7.85 (m, 2 H, H-4′ and H-5′); 7.46 (dd, J = 1.6 and 7.2 Hz, 1 H, H-3′); 7.10 (d, J = 9.2 Hz, 2 H, H-1 and H-8); 7.01 (d, J = 9.2 Hz, 2 H, H-2 and H-7); 3.64 (s, 3 H, OCH_3) ppm; IR (KBr): ν_{max} 3500–300 (NH stretch); 1725 (CO stretch); 1636; 1587; 1539; 1449; 1401; 1333; 1276; 1202 cm^{-1}; LRMS (FAB): m/z 501; 503; 505 (relative intensities: 38:77:41); UV–visible (CH_3OH): λ_{max} 511 nm.

Rhodamine n*-butyl ester (dye 4).* Rhodamine 110 (631.2 mg; 1.72 mmol) was suspended in *n*-butanol (50 mL) in a 100 mL three necked round-bottom flask equipped with a condenser and a drying tube containing anhydrous $CaSO_4$. Hydrochloric acid gas was bubbled through the solution for 45 min. The rhodamine 110 did not completely dissolve. The reaction mixture was stirred 23 h at room temperature, refluxed for 3 h, stirred again at room temperature overnight and then refluxed for an additional 5 h. *n*-Butanol was evaporated under reduced pressure and a dark brown solid residue was obtained. The residue was purified by column chromatography using dichloromethane and increasing concentration of methanol as eluent. Evaporation of fractions containing rhodamine *n*-butyl ester afforded a brown residue that was purified by a second column chromatography using dichloromethane–methanol (80:20) as the sole eluent. Evaporation of fractions containing the product gave a red-brown solid that was kept under reduced pressure until its weight remained constant. Rhodamine *n*-butyl ester (dye **4**) (511 mg) was obtained with a 70% yield. The product was used without further purification as starting material in the next step of the synthesis. ^{1}H RMN (300 MHz, CD_3OD): δ 8.29 (dd, J = 1.6 and 7.4 Hz, 1 H, H-6′); 7.82 (m, 2 H, H-4′ and H-5′); 7.42 (dd, J = 1.6 and 7.2 Hz, 1 H, H-3′); 7.05 (d, J = 8.7 Hz, 2 H, H-1 and H-8); 6.83 (d, J = 2.1 Hz, 2 H, H-4 and H-5); 6.81 (dd, J = 2.1 and 8.7 Hz, 2 H, H-2 and H-7); 3.95 (t, J = 6.2 Hz, 2 H, $OCH_2CH_2CH_2CH_3$); 1.25 (m, 2 H, $OCH_2CH_2CH_2CH_3$); 0.99 (m, 2 H, $OCH_2CH_2CH_2CH_3$); 0.76 (t, J = 7.3 Hz, 3 H, $OCH_2CH_2CH_2CH_3$) ppm; UV–visible (CH_3OH): λ_{max} 545 nm.

4,5-Dibromorhodamine n*-butyl ester (dye 3).* Rhodamine *n*-butyl ester (509 mg; 1.20 mmol) was dissolved in anhydrous ethanol (50 mL) in a round-bottom flask equipped with a condenser. A fresh bromine solution was prepared in a separate vessel by dissolving Br_2 (1.5 mL) in anhydrous ethanol (100 mL). A portion of this ethanolic bromine solution (8.3 mL; 2.42 mmol of Br_2) was added to the rhodamine 110 *n*-butyl ester solution. The reaction mixture was stirred at room temperature for 71.5 h. The progression of the reaction was monitored by chromatography and two additional portions of fresh bromine solution (2.1 mL; 0.61 mmol of Br_2 and 1.0 mL; 0.27 mmol of Br_2), each followed by 1 h of stirring at room temperature, were necessary to bring the reaction to completion. Evaporation of the reaction mixture under reduced pressure gave a dark red solid residue. The residue was dissolved in ethanol and evaporated again to dryness five times to make sure that any trace of Br_2 was removed. The residue was pumped under vacuum (0.025 mm Hg) for 13 h at room temperature and for 21 h at 110°C (0.025 mm Hg) in an Abderhalden drying pistol using anhydrous $CaSO_4$ as drying agent. 4,5-Dibromorhodamine *n*-butyl ester (dye **3**) was obtained in a quantitative yield (purity >99% by HPLC). ^{1}H RMN (300 MHz, CD_3OD): δ 8.31 (dd, J = 1.7 and 7.5 Hz, 1 H, H-6′); 7.84 (m, 2 H, H-4′ and H-5′); 7.46 (dd, J = 1.8 and 6.9 Hz, 1 H, H-3′); 7.12 (d, J = 9.2 Hz, 2 H, H-1 and H-8); 7.03 (d, J = 9.2 Hz, 2 H, H-2 and H-7); 3.95 (t, J = 6.2 Hz, 2 H, $OCH_2CH_2CH_2CH_3$); 1.22 (m, 2 H, 2 H, $OCH_2CH_2CH_2CH_3$); 0.93 (m, 2 H, 2 H, $OCH_2CH_2CH_2CH_3$); 0.75 (t, J = 7.3 Hz, 3 H, 2 H, $OCH_2CH_2CH_2CH_3$) ppm; IR (KBr): ν_{max} 3500–300 (NH stretch); 1697 (CO stretch); 1638; 1589; 1536; 1453; 1403; 1334; 1303; 1203 cm^{-1}; LRMS (FAB): m/z 543; 545; 547 (relative intensities: 25:49: 26); UV–visible (CH_3OH): ν_{max} 511 nm.

The SMF-AI rhabdomyosarcoma cell line were obtained from F. Babai and established in culture as described previously (15). The K562 and RAT-2 cell lines were obtained from the American Type Culture Collection (Rockville, MD) and passaged as recommended. The EM2 cell lines were a generous gift from A. Keating and were maintained as previously described (16).

HPLC analysis

The purity of the synthesized dyes was assessed by HPLC. The system used combines an Alcott 728 autosampler, a Rheodyne injector with a 50 μL loop, a Hitachi L-6200 system controller and pump, a Jasco UV-975 Intelligent UV–visible detector and a Shimadzu CR501 Chromatopac electronic integrator. We used a reverse-phase Radial-Pak Prep Nova-Pak HRC18 column from Waters (8 × 100 mm, 6 μm particle size, 60 Å pore size). The composition of the mobile phase was CH_3OH–H_2O–CH_3COOH (60–38–2)% vol/vol and the flow rate 2.0 mL/min. Samples were prepared by dissolving dyes **1** **2** and **3** in spectrograde methanol (0.5 mg/mL). Two different wavelengths of detection were used (510 and 254 nm). Purity of the dyes used in this study was, in all cases, found to be superior to 99% by this method.

Spectroscopy studies

The absorption spectra were recorded on a Philips PU-8800 UV–visible spectrophotometer. Corrected fluorescence spectra were recorded on a Spex Fluorolog-2 spectrofluorometer with an F2T11

special configuration. Fluorescence lifetimes were measured on a multiplexed time-correlated single-photon counting fluorometer (Edinburgh Instruments, model 299T). Details of the instrumental setup are described elsewhere (17). For spectroscopic measurements the dye concentration was always kept below 1×10^{-6} mol dm^{-3} in order to avoid dye aggregation and to minimize the reabsorption effect. To avoid any aggregation we check that the Beer–Lambert law is valid in the concentration range we have studied. Freshly prepared solutions were always used. Samples were not degassed because oxygen does not quench the S_1 excited state of rhodamines. However it is also preferable not to degas the solutions as oxygen inhibits the photodecomposition of rhodamines (18). All fluorescence quantum yields were measured using zwitterionic rhodamine B in methanol ($\phi_f = 0.53$) as a standard (18). In all cases, the fluorescence excitation spectra exactly match the absorption spectra of the dyes. This is considered to be the best purity criteria in fluorescence spectroscopy.

For singlet oxygen emission measurement the oxygen-saturated solution of the dye was excited at 514.5 nm with an argon-ion laser and the emission was detected at right angles to the direction of the excitation. The detector system was an ultrasensitive near-IR spectrophotometer based on a Spex 500M monochromator equipped with a 600 lines/mm grating blazed at 1 μm and controlled with an MSD controller, liquid nitrogen-cooled Ge detector (model ADC 403L, Applied Detector Co.) followed by a Stanford Research SR510 lock-in-amplifier. An optical chopper (Stanford Research SR540) was placed in front of the monochromator entrance slit. The amplifier and the controller were interfaced to an MS-DOS personal computer where the data are collected. To avoid photobleaching of these dyes under strong illumination of the laser, a flow system of the dye solution using a peristaltic pump, a flow cell (Precision Cell Inc.) and teflon fluororubber tubing was used (19). Quantum yields of sensitized (photooxygenated) singlet oxygen by rhodamine dyes were estimated relative to the (photoquantum) yield of singlet oxygen generated by rose bengal in methanol reported to be 0.8 (20).

Photosensitization in different cell lines

Cell Preparation for PDT. Cells were passaged 2 days before the experiment. On the day of the experiments, cells were incubated at a concentration of 5–20 $\times 10^6$ cells per 100 mm petri dish for 40 min in complete media with 10% serum and 25 μmol of dye **1**, **2** or **3**. After two washes, cells were allowed a 1 h extrusion time in fresh media before irradiation with the diverged beam of 514.5 nm wavelength of the Coherent Innova 15 W argon-ion laser. Adherent cells were seeded at 500–1000 cells per 100 mm petri dishes and colonies were scored 7 days posttreatment. Exposure time necessary for the specific energy was calculated using a power meter (Coherent 210). After PDT, cells were incubated without further manipulations, and cell viability or colony growth was assessed at different times.

Cell viability and colony formation. Colonies were visually scored at 40× magnification on an Olympus IMT-2 inverted microscope. Cell viability was assessed using trypan blue dye exclusion. Duplicate counts were averaged for each sample in each experiment.

RESULTS AND DISCUSSION

Chemical synthesis of the new dibrominated rhodamine dyes

The synthesis of the new dibrominated rhodamine dyes **2** and **3** used in this study was accomplished as illustrated in Scheme 1.

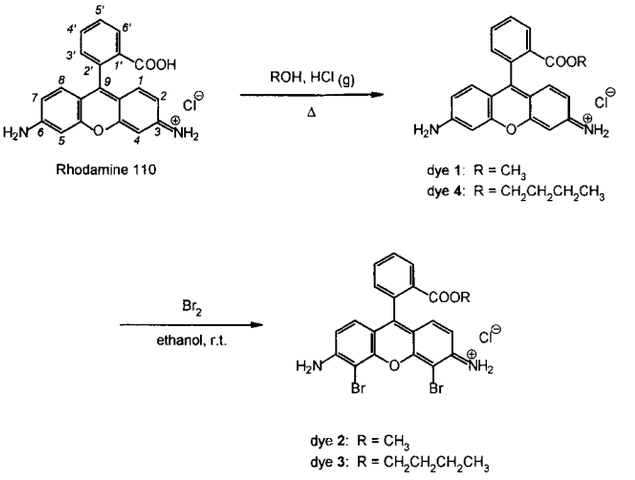

Scheme 1. Synthesis and structure of dyes **1**, **2** and **3**.

Rhodamine methyl ester (rhodamine 123) (dye **1**) and rhodamine *n*-butyl ester (dye **4**) were first prepared by refluxing rhodamine 110 in the appropriate alcohol in which HCl gas had been dissolved. Both rhodamine esters were purified by flash chromatography using dichloromethane and increasing concentrations of methanol as eluent. The structures of both products was confirmed by the appearance of signals generated by the protons of the corresponding alkoxy moieties in the ^{1}H NMR spectra of the esters. In addition, the ^{1}H NMR spectrum of dye **1** is identical to that of commercially available rhodamine 123. Both rhodamine esters were then dibrominated at room temperature using dilute solutions of bromine in ethanol. The progression of the bromination reaction was followed by chromatography and additional portions of bromine solution were added until the transformation was quantitative. Under these conditions, the reaction stops after addition of two bromine atoms at positions 4 and 5 of the rhodamine system and no tribrominated or tetrabrominated products are formed. In separate experiments, we have found that tetrabromination of rhodamine derivatives can be achieved by refluxing in a large excess of neat bromine. The fact that dibromination of the rhodamine esters occurs solely at positions 4 and 5 was clearly established by analysis of the coupling patterns observed in the ^{1}H NMR spectra of the dibrominated dyes **2** and **3**. The signals generated by the two groups of protons at positions 1,8 and 2,7 are clearly resolved. These signals appear as doublets with an *ortho* coupling constant of 9.2 Hz. This coupling pattern cannot be generated by any other regioisomer. Finally, the presence of two bromine atoms on the rhodamine system is also confirmed by the typical isotopic distribution pattern of the molecular ions observed in the mass spectra of dyes **2** and **3**.

The purity of rhodamine dyes **1**, **2** and **3** used in this study was assessed by HPLC. Baseline resolution was achieved using a C18 reverse-phase column and a mixture of methanol, water and acetic acid (60:38:2) as mobile phase. Two different wavelengths were used for detection. A wavelength of 510 nm was used because it provides maximum sensitivity for the detection of rhodamine derivatives. A wavelength of 254 nm was also used to confirm the absence of non-

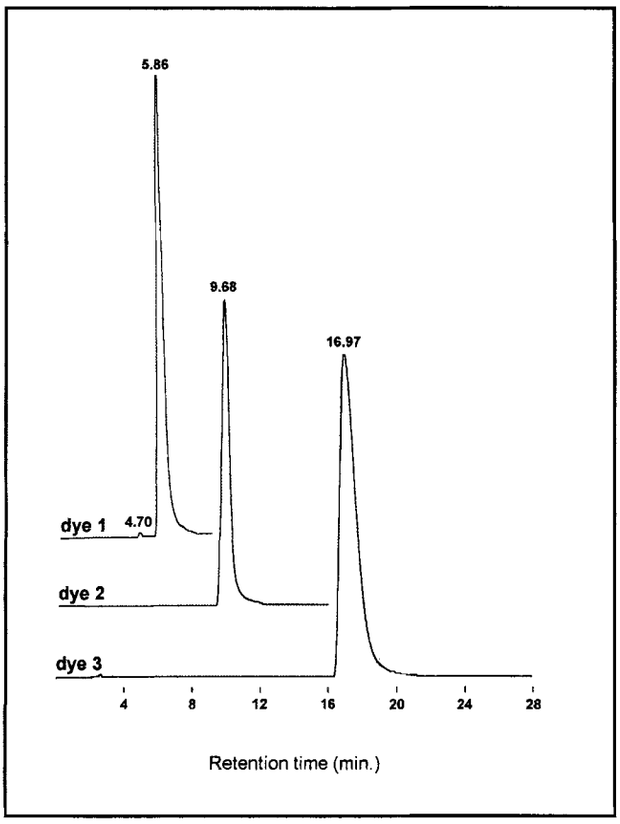

Figure 1. Chromatograms (HPLC) of dyes **1**, **2** and **3** (0.5 mg/mL in methanol; 50 μL injection volume) recorded ($\lambda_{det.}$ = 510 nm) using a reverse-phase Radial-Pak Prep Nova-Pak HRC18 column from Waters (8 × 100 m*M*, 6 μm particle size, 60 Å pore size). The composition of the mobile phase was CH_3OH–H_2O–CH_3COOH (60-38-2) % vol/vol and the flow rate 2.0 mL/min.

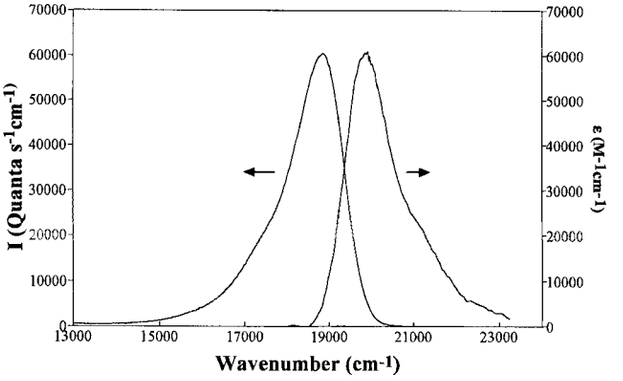

Figure 2. Room temperature absorption and fluorescence spectra of dye **2** in H_2O. Fluorescence intensity is in relative units.

rhodamine impurities. The chromatograms of dyes **1**, **2** and **3** are shown in Fig. 1 ($\lambda_{det.}$ = 510 nm). Chromatograms obtained with a detection wavelength of 254 nm do not show any additional peak beside the injection peak. The purity of dyes **1**, **2** and **3** was found, in all cases, to be superior to 99% using this method. Only the chromatogram of dye **1** shows a detectable impurity at retention time of 4.70 min, consisting of less than 1% of residual rhodamine 110.

Spectroscopic properties

We have studied the absorption and emission spectra of dyes **1**, **2** and **3** in water, methanol, ethanol and also in SDS micelles. Figure 2 shows the representative absorption and emission spectra of dye **2** in water. Table 1 shows details of the spectral features of these dyes in different media. From the table it is evident that due to bromination, absorption and emission maxima are only slightly red-shifted by about 200 cm^{-1}. It is observed that for the three dyes, the absorption and emission maxima are shifted to the blue with a concomitant general broadening of the bands going from ethanol to water. This result is opposite to a normal solva-

Table 1. Spectroscopic data for different rhodamine dyes at 293 K

Sample	Solvent	$\bar{\nu}_A$*	ε† (M^{-1} cm^{-1})	$FWHM_A$‡ (cm^{-1})	$\bar{\nu}_F$§ (cm^{-1})	$FWHM_F$ (cm^{-1})	Stokes shift (cm^{-1})
1	H_2O	20 080	60 700	1400	19 030	1600	1050
	MeOH	19 880	82 100	1160	18 960	1450	920
	EtOH	19 720	85 700	1180	18 850	1360	870
	SDS (0.05 *M*)	19 720	57 900	1260	18 800	1490	920
2	H_2O	19 840	60 500	1420	18 830	1500	1010
	MeOH	19 590	74 000	1200	18 660	1340	930
	EtOH	19 490	72 500	1230	18 570	1110	820
	SDS (0.05 *M*)	19 530	71 500	1370	18 570	1420	960
3	H_2O	19 800	60 700	1350	18 830	1400	970
	MeOH	19 590	73 100	1200	18 690	1300	900
	EtOH	19 460	74 100	1190	18 590	1200	870
	SDS (0.05 *M*)	19 650	60 500	1340	18 690	1430	960

*Absorption wavenumbers at the peak intensity maximum.
†Absorption coefficients at the peak intensity maximum.
‡FWHM = full width at half maximum.
§Fluorescence wavenumbers taken at the peak intensity maximum.

Table 2. Photophysical properties of different rhodamine dyes

Sample	Medium	ϕ_F	τ_F (ns) 295 K	τ_F (ns) 77 K	$k_F \times 10^{-8}$ (s^{-1})	$k_{nr} \times 10^{-7}$ (s^{-1})	$k_{ic} \times 10^{-7}$ (s^{-1})	$k_{isc} \times 10^{-7}$ (s^{-1})	ϕ_T*	ϕ_Δ
1	H_2O	0.87	4.2	3.4	2.1	3.1				
	MeOH	0.86	4.2	3.5	2.1	3.3				
	EtOH	0.86	4.0		2.2	3.5				
	SDS (0.05 *M*)	0.83	4.7		1.8	3.6				
2	H_2O	0.34	1.6	2.6	2.1	40.2	24	16	0.27	0.30
	MeOH	0.56	2.4		2.3	18.3				0.47
	EtOH	0.52	2.5	2.9	2.1	19.5	5.5	14	0.36	0.40
	SDS (0.05 *M*)	0.35	2.1		1.7	31.4				0.44
3	H_2O	0.32	1.6	2.7	2.0	43.3	25	18	0.29	0.30
	MeOH	0.48	2.4		2.0	21.8				0.51
	EtOH	0.47	2.4	2.9	2.0	22.3	6.5	16	0.38	0.43
	SDS (0.05 *M*)	0.39	2.1		1.9	29.8				0.44

*Calculated triplet quantum yield following Eq. 1.

tochromic effect where the excited state is more stabilized in a more polar solvent giving rise to red-shifted emission bands. This result indicates the hydrogen-bonding capability of the amino end group of the dyes, which increases with the increasing proton donor ability of protic solvents. This is a well-known phenomenon occurring in aromatic amines, which is attributed to the hydrogen-bonding interaction (more important in water than in alcohols) involving the lone pair of the terminal nitrogen atom. This is called the blue shift anomaly observed for amino molecules dissolved in protic solvents (21–23). The protic solvent acts as a hydrogen bond donor to the lone pair of the terminal amino group causing a reduced conjugation with the aromatic moiety. In some cases, this has the consequence of reducing the planarity of the whole molecular skeleton in the ground and relaxed electronic excited states. Consequently, the absorption and fluorescence bands are broadened accordingly. Table 1 shows that this is indeed the case, the absorption and fluorescence bandwidths generally increase going from ethanol to water. Even though the change is rather small, it might help elucidate the average site of these dyes in microheterogeneous systems like SDS.

Photophysical properties

Table 2 shows the photophysical properties of these dyes. For dye **1**, ϕ_F is very high and is found to be nearly independent of the solvent at room temperature. ϕ_F of dye **1** in water at room temperature is quite similar to that reported (0.9) by other workers (24). The fluorescence lifetime τ_F is also approximately constant going from water to ethanol. We have also calculated the radiative rate constant k_F ($=\phi_F/\tau_F$) and the nonradiative rate constant k_{nr} ($=[1 - \phi_F]/\tau_F$). The k_{nr} may consist of two parts when photochemistry is absent. One is k_{isc}, the rate constant for intersystem crossing and the other is k_{ic} the rate constant for internal conversion ($k_{nr} = k_{isc} + k_{ic}$). For dye **1** it is found that both k_f and k_{nr} are independent of the solvent nature. For dyes **2** and **3**, ϕ_F decreases appreciably in water. The same trends are also observed for τ_F. For all these dyes k_F values are almost the same. But upon bromination the k_{nr} value increases drastically. It is likely that bromination increases the efficiency of intersystem crossing to the triplet manifold *via* spin-orbital coupling. Therefore, the increase in k_{nr} value would reflect the increase in the triplet quantum yield. At room temperature, ϕ_F for dye **2** and for dye **3** in water are much less than that in methanol and ethanol in contrast with the similar values for dye **1**. It is well known that rhodamines with rigid amino groups (rhodamine 101) or rhodamines in frozen solutions show fluorescence quantum yields close to 1 (24,25). The rate constants of the internal conversion from the S_1 excited state of rhodamines increase strongly upon alkylation of the amino groups (25–28), leading to important decreases in the fluorescence lifetimes and quantum yields. On the basis of these results, intramolecular rotation of the amino fragments was proposed as the main pathway for the nonradiative deactivation from the S_1 excited state of rhodamines (25,28). Moreover, it has been reported (26) that the internal conversion due to the formation of twisted intramolecular charge transfer (TICT) states originating from the rotation of amino or monoethyl amino groups in xanthene dyes is not possible. Only the TICT state of diethyl or higher amino group is energetically lower than the S_1 state. An alternative mechanism for internal conversion of rhodamines has recently been considered (29). This mechanism correlates internal conversion with a change in the amino groups from a planar structure (xanthene=N^{+}<) to a pyramidal one (xanthene^{+}–$\ddot{N}$>), the so-called open–closed umbrella-like motion (30). This structural change involves disruption of the xanthene–amine double bonds to a xanthene–amine single bond (now the amine group can freely rotate) and displacement of a rhodamine positive charge from the amino N atom to the xanthene ring. In dye **2** and in dye **3** the presence of the bromine atom in the xanthene moiety may facilitate the above type of charge transfer and this process would dominate in water.

We have found that ϕ_F and τ_F for dye **2** and dye **3** are the same in higher viscous alcohols such that the above process may be insignificant in these media. To clarify this point we measure the τ_F in water and in ethanol at 77 K. Fluorescence decay profiles of dye **2** in water at room temperature and at

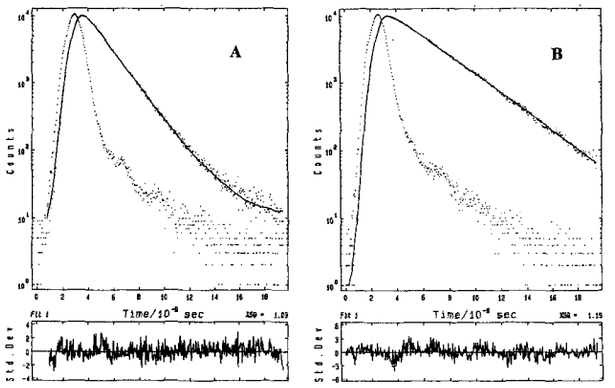

Figure 3. Fluorescence decay curves associated with the lamp profile showing the single exponential decay of dye **2** in water at 295 K (A) and at 77 K (B). λ_{exc} = 480 nm and λ_{em} = 530 nm.

77 K are shown in Fig. 3. It is found that in water, τ_F changes appreciably. It increases to 2.7 ns from 1.6 ns. The values are given in Table 2. But in ethanol this change is small. Assuming that the rotation of the amino group is frozen at 77 K and also that the singlet–triplet energy gap is about the same at room temperature and at 77 K, *i.e.* k_F and k_{isc} are independent of temperature, then k_{ic} can be calculated according to $k_{ic} = (1/\tau_F) - (1/\tau_F^{77})$ and consequently, knowing k_{ic} and k_{nr} one can evaluate k_{isc} at room temperature. Values of k_{ic} and k_{isc} are given in Table 2. The triplet quantum yield ϕ_T can be calculated using the formula:

$$\phi_T = \frac{k_{isc}}{k_f + k_{ic} + k_{isc}}. \quad (1)$$

Calculated values of ϕ_T are given in Table 2. The results indicate that the internal conversion due to rotation of the amino group dominates in water. Within the limit of experimental error, the intersystem crossing quantum yield is less in water for both dyes.

We have also studied the spectroscopic and photophysical properties of these dyes in a micellar medium. Results are tabulated in Tables 1 and 2. As the dyes are cationic, we use the anionic micelle (0.05 *M* SDS) in water (critical micelle concentration = 8.0×10^{-3} mol dm^{-3}) (31) to monitor the solubilization behavior and the dye–micellar interaction. Absorption and emission maxima indicate that dye **1** and dye **2** are solubilized in SDS and are facing ethanolic-like media. A small but distinct decrease in k_F indicates that there may be some weak complex formation for dyes **1** and **2**. Dye **3** behaves slightly differently. Its penetration inside the micelle is definitely hampered. The bulky substituent *n*-butyl ester group is likely to play a certain role here as far as the solubilization of the dyes in SDS micelles is concerned.

Singlet oxygen quantum yield determination

We have determined the singlet oxygen quantum yield sensitized by these dyes in water, methanol, ethanol and in SDS relative to rose bengal in methanol as a standard. We have used the following equation (32):

$$\phi_\Delta = \phi_\Delta^{st} \frac{I\,(1 - 10^{-A_{514.5}^{st}})\,n^2\,k_\Delta^{st}}{I^{st}\,(1 - 10^{-A_{514.5}^{st}})\,n_{st}^2\,k_\Delta} \quad (2)$$

where st represents the standard, ϕ_Δ is the singlet oxygen quantum yield, I is the area under the 1268 nm singlet oxygen emission band, $A_{514.5}$ is the absorbance at the wavelength of excitation (514.5 nm), k_Δ^{st} is the radiative rate constant for singlet oxygen emission in methanol for rose bengal, k_Δ is the radiative rate constant for singlet oxygen emission in the solvent investigated for the particular sample and n is the refractive index of the solvent.

The values of

$$\frac{k_\Delta^{MeOH}}{k_\Delta^{C_6H_6}}, \frac{k_\Delta^{H_2O}}{k_\Delta^{C_6H_6}} \text{ and } \frac{k_\Delta^{EtOH}}{k_\Delta^{C_6H_6}} \quad (3)$$

are already reported in the literature (33) and are 0.18, 0.05 and 0.26, respectively. We have used these values to calculate

$$\frac{k_\Delta^{MeOH}}{k_\Delta^{H_2O}} \text{ and } \frac{k_\Delta^{MeOH}}{k_\Delta^{EtOH}} \quad (4)$$

from the following known ratios

$$\frac{k_\Delta^{MeOH}}{k_\Delta^{C_6H_6}} \Big/ \frac{k_\Delta^{H_2O}}{k_\Delta^{C_6H_6}} \text{ and } \frac{k_\Delta^{MeOH}}{k_\Delta^{C_6H_6}} \Big/ \frac{k_\Delta^{EtOH}}{k_\Delta^{C_6H_6}} \quad (5)$$

respectively.

The ratios in expression 4 are 5.2 and 0.69, respectively. For SDS we used the value of water because the singlet oxygen lifetimes in D_2O and in 10 m*M* SDS in D_2O are reported to be identical (34). We assume that a similar phenomenon will be observed in H_2O also. The values of ϕ_Δ obtained are given in Table 2. For dye **1** we were unable to detect any singlet oxygen emission. For dye **2** and dye **3**, the quantum yields are found to be higher in methanol, ethanol and in SDS as compared to water. The values of calculated triplet quantum yields (ϕ_T) and singlet oxygen quantum yield (ϕ_Δ) indicate that in water and in ethanol the energy transfer from the triplet state of the dyes to singlet oxygen is almost 100% because within the limit of experimental error, ϕ_T is approximately equal to ϕ_Δ. In water, ϕ_Δ values are slightly less compared to other media. This is due to the higher internal conversion in this strongly protic medium as discussed above.

Leukemic cell line photosensitization

Although dye **1** has been used as a PS, high energies in the range of 300 J/cm^2 were necessary to achieve cell killing. Lower energy levels (1–10 J/cm^2) were used in our experiments. The AI and RAT-2 cells were plated either alone or mixed together (50/50) in 100 mm petri dishes. Discriminatory colony counting of mixtures of AI and RAT-2 cells after PDT were possible because the AI cell line had previously been transfected with a β-galactosidase expression vector allowing for a specific blue coloration of the AI colonies, therefore distinguishing them from RAT-2 cells. Figure 4A shows that dye **1** is a poor PS for high (SMF-AI) or low (RAT-2) retention cell lines. Figure 4B shows specific inhibition of AI cell colony formation at energies in the range of 2–5 J/cm^2 using dye **2** as PS. Minimal toxic effect from AI photoeradication is exerted on RAT-2 cells upon PDT as the RAT-2 cell colony survival, size and appearance in mixed cultures with AI are comparable to monoculture of RAT-2 (Fig. 4B). This could indicate that no major toxic by-

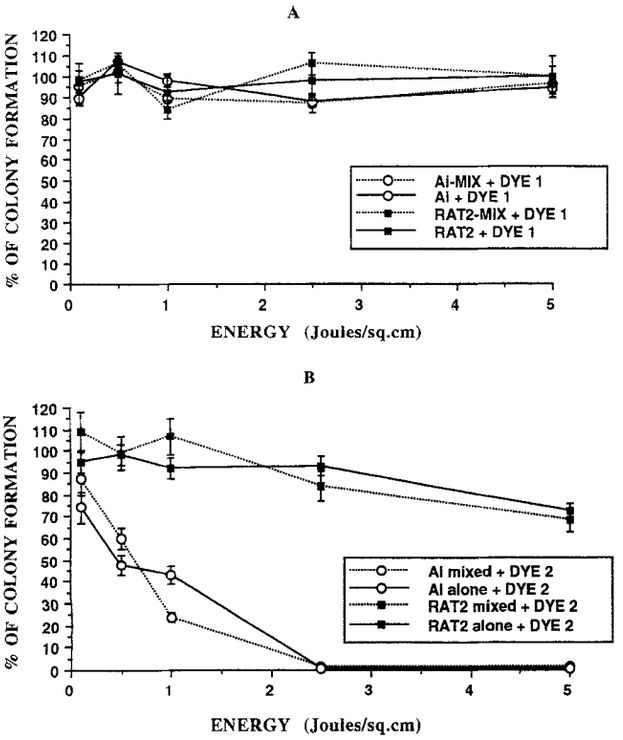

Figure 4. Colony formation of RAT-2, AI and 50/50 mixtures of RAT-2 and AI cells at different times after PDT with energies varying from 0.1 to 5 J/cm^2. The RAT-2 and AI cells were either plated alone (RAT-2 alone + dye, AI alone + dye), or in equal mixtures in which colony formation of RAT-2 (RAT-2-mixed + dye) and AI (AI-mix + dye, blue colonies) were assessed simultaneously. A: Colony counts after incubation with dye **1** and PDT. B: Colony counts after incubation with dye **2**.

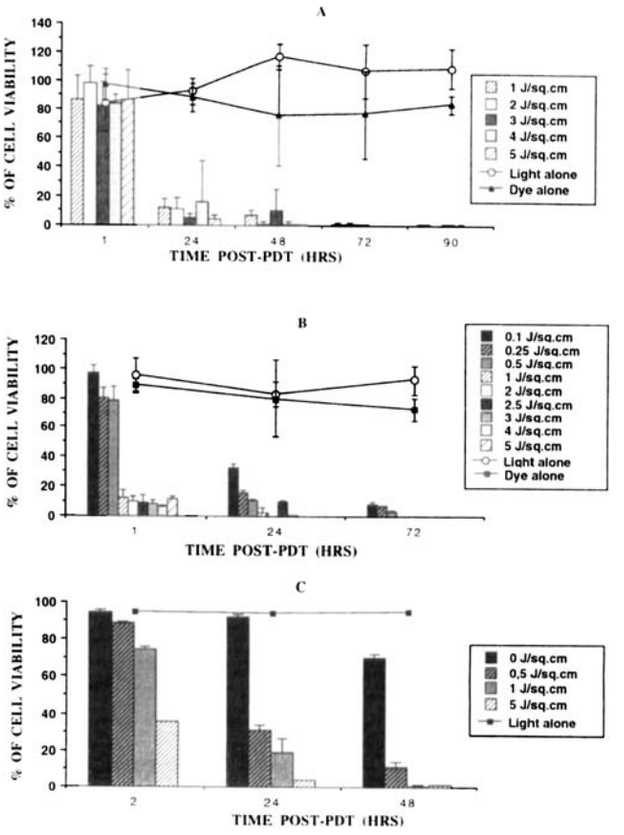

Figure 5. Cell viability assessed by trypan blue exclusion of suspension cultures of leukemic cell lines at different times after PDT. A: The K562 cell line incubated with dye **2**. B: The EM-3 leukemic cell line incubated with dye **2**. C: The K562 cell line incubated with dye **3**. Data are averaged for a series of seven experiments.

product of AI PDT is acting on "innocent bystanders" during and after PDT.

Rhodamine 123 has been shown to be bound to the multidrug transporter gene family (MDR) (35,36). We used an MDR-positive leukemic cell line K562 in combination with dye **2** incubation as a target for PDT. Energies in the range previously shown to spare low retention and kill high retention cells were used. It is shown in Fig. 5A that cell viability of the MDR cell line K562 is significantly decreased in culture at energies in the range of 1–5 J/cm^2. Dye **1** has no effect on cell viability under similar experimental conditions (results not shown). The chronic myelogeneous leukemia cell line EM2 is shown in Fig. 5B to be more sensitive to similar PDT conditions as cell viability is dramatically lowered after 1 h of culture. The K562 cells need higher energy and longer post-PDT time to reduce the cell viability significantly. Figure 5C shows that dye **3** is also a potent PS as K562 cell viability decreases significantly 2 h post-PDT using the same conditions. The main disadvantage with dye **3** is that it is more intrinsically toxic (results not shown) than dye **2**. Our fluorescence-activated cell sorting data (not shown) indicate that dye uptake and extrusion rate are slower with dye **3**. These cationic dyes are known to be accumulated preferentially at negatively charged mitochondrial membranes, consistent with the dye subcellular distribution observed using fluorescence microscopy. The slower extrusion kinetics, which may be the primary cause for intrinsic toxicity, are probably due to the presence of a longer aliphatic side chain. Our spectroscopic and photophysical studies in anionic SDS micelles also reveal a similar situation.

CONCLUSIONS

Two new dyes were synthesized. Spectroscopic properties of these dyes and of rhodamine 123 in protic solvents indicate the hydrogen-bonding capability of the amino end group lone pair of these dyes, which increases with the increasing proton donor ability of the solvents. As far as the solubilization of these dyes in SDS micelle is concerned the bulkiness of the ester group plays a dominant role.

Photophysical properties of these dyes indicate that due to bromination, intersystem crossing quantum yield increases. At room temperature, internal conversion due to rotation of the amino group dominates in water. No singlet oxygen quantum yield (ϕ_Δ) is observed for the unbrominated dye **1**. Calculated ϕ_T and ϕ_Δ values indicate that the energy transfer from triplet state of dyes **2** and **3** to singlet oxygen is almost 100%. The fact that the singlet oxygen quantum yield is higher in SDS than in water shows some promise, for these probes solubilized in heterogeneous media like membranes, in PDT.

Dye **2** was shown to be a potent PS for the eradication of

neoplastic cells of different origins. At low doses of light, 24–48 h are necessary for significant decreases in cell viability. Dye **3** is also a good PS but has more intrinsic toxicity than dye **2**. Dye **1** has no PDT effects in the energy range of 1–5 J/cm^2. These observations together with the singlet oxygen quantum yield data predict that singlet oxygen photosensitization is the primary step for photodynamic action. Under a mixed culture environment, minimal toxic effect from AI photoeradication is exerted on RAT-2 cells upon PDT as the RAT-2 cell colony survival, size and appearance in mixed cultures with AI are comparable to monocultures of RAT-2.

Acknowledgements—The authors thank Professor C. Reber for the use of his near IR spectrophotometer. This work was supported by a grant from Theratechnologies Inc., Montréal, Québec, Canada.

REFERENCES

1. Lipson, R. L., M. J. Gray and E. J. Baldes (1966) Hematoporphyrin derivative for detection and management of cancer. Proceeding IX International Cancer Congress, 393.
2. Dougherty, T. J. (1974) Activated dyes as antitumor agents. *J. Natl. Cancer Inst.* **51**, 1333–1336.
3. Dougherty, T. J., C. J. Gomer and K. R. Weishaupt (1976) Energetics and efficiency of photoinactivation of murine tumor cells containing hematoporphyrin. *Cancer Res.* **36**, 2330–2333.
4. Dougherty, T. J., J. E. Kaufman, A. Goldborg, K. R. Weishaupt, D. Boyle and A. Mittleman (1978) Photoradiation therapy for the treatment of malignant tumors. *Cancer Res.* **38**, 2628–2635.
5. Khan, A. U. and M. Kasha (1979) Direct spectroscopic observation of singlet oxygen emission at 1268 nm excited by sensitizing dyes of biological interest in liquid solution. *Proc. Nat. Acad. Sci. USA* **76**, 6047–6049.
6. Kessel, D. and E. J. Dutton (1984) Photodynamic effects: porphyrin *vs* chlorin. *Photochem. Photobiol.* **40**, 403–405.
7. Dougherty, T. J., K. P. Weishaupt and D. G. Boyle (1985) Photodynamic sensitizer. In *Cancer: Principle and Practice of Oncology,* 2nd ed. (Edited by V. T. DeVite, S. Hellman and S. Rosenberg), pp. 2272–2279. J. B. Lippincott, Philadelphia.
8. Nelson, J. S., W. G. Roberts and M. W. Berns (1987) *In vivo* studies on the utilization of mono-L-aspartyl chlorin (NPe6) for photodynamic therapy. *Cancer Res.* **47**, 4681–4685.
9. Summerhayes, I. C., T. J. Lampidis, S. D. Bernal, J. I. Nadakavukaren, K. K. Nadakavukaren, E. L. Shepherd and L. B. Chen (1982) Unusual retention of rhodamine 123 by mitochondria in muscle and carcinoma cells. *Proc. Nat. Acad. Sci. USA* **79**, 5292–5296.
10. Modica-Napolitano, J. S., M. J. Weiss, L. B. Chen and J. R. Aprille (1984) Rhodamine 123 inhibits bioenergetic function in isolated rat liver mitochondria. *Biochem. Biophys. Res. Commun.* **118**, 717–723.
11. Chow, A., J. Kennedy, R. Pottier and T. G. Truscott (1986) Rhodamine 123—photophysical and photochemical properties. *Photochem. Photobiophys.* **11**, 139–148.
12. Morliere, P., P. Santus, M. Bazin, E. Kohen, V. Carillet, F. Bon, J. Rainasse and L. Dubertret (1992) Is rhodamine 123 a photosensitizer? *Photochem. Photobiol.* **52**, 703–710.
13. Lin, C. N. (1990) *Selective Localization of Photosensitizer in Humans,* Vol. 11, pp. 79–101. CRS Press, Boca Raton, FL.
14. Sarpal, R. S., M. Belletête and G. Durocher (1993) Fluorescence probing and proton transfer equilibrium reactions in water, SDS and CTAB using 3,3-dimethyl-2-phenyl-3H-indole. *J. Phys. Chem.* **97**, 5007–5013.
15. Babai, F. and A. Royal (1994) Rat myoblastic sarcoma cell lines. A model for the study of invasion, metastasis, and myogenic differentiation. *Lab. Invest.* **70**, 907–915.
16. Keating, A., P. J. Martin, I. D. Berstein, T. Papayonnopoulou, W. Raskind and J. W. Singer (1983) *EM-2 and EM-3: Two New PH1 + Myeloid Cell Lines. Normal and Neoplastic Hematopoiesis,* pp. 513–520. Alan R. Liss, New York.
17. Zelent, B., T. Ganguly, L. Farmer, D. Gravel and G. Durocher (1991) Studies on the photophysical properties of some 2,7-dimethoxycarbazoles in various environments by steady state and time resolved spectroscopic methods: part 1. Synthesis, absorption and fluorescence spectra at room temperature. *J. Photochem. Photobiol. A Chem.* **56**, 165–181.
18. Snare, M. J., F. E. Treloar, K. P. Ghiggino and P. J. Thistlewaite (1982) The photophysics of rhodamine B. *J. Photochem.* **18**, 335–346.
19. Hall, R. D. and C. F. Chignell (1987) Steady-state near-infrared detection of singlet molecular oxygen: a Stern–Volmer quenching experiment with sodium azide. *Photochem. Photobiol.* **45**, 459–464.
20. Wilkinson, F., W. P. Helman and A. B. Ross (1993) Quantum yields for the photosensitized formation of the lowest electronically excited singlet state of molecular oxygen in solution. *J. Phys. Chem. Ref. Data* **22**, 113–262.
21. Suppan, P. (1968) Solvent effects on the energy of electronic transition: experimental observations and applications to structural problems of excited molecules. *J. Chem. Soc. (A),* 3125–3133.
22. Belletête, M., S. Nigam and G. Durocher (1995) Conformational analysis and electronic spectroscopy of donor–acceptor 3H-indole derivatives in nonaqueous media: combined experimental and theoretical approach. *J. Phys. Chem.* **99**, 4015–4024.
23. Belletête, M., R. S. Sarpal and G. Durocher (1994) Photophysics of some substituted 3H-indole probe molecules and their charged species. *Can. J. Chem.* **72**, 2239–2248.
24. Kubin, R. F. and A. N. Fletcher (1982) Fluorescence quantum yields of some rhodamine dyes. *J. Lumin.* **27**, 455–462.
25. Drexhage, K. H. (1973) In *Dye Laser* (Edited by F. P. Schafer), p. 144. Springer, Berlin.
26. Vogel, M., W. Rettig, R. Sens and K. H. Drexhage (1988) Structural relaxation of rhodamine dyes with different N-substitution patterns: a study of fluorescence decay times and quantum yields. *Chem. Phys. Lett.* **147**, 452–460.
27. Osborne, A. D. and A. C. Winkworth (1982) Viscosity dependent internal conversion in an aryl-substituted rhodamine dye. *Chem. Phys. Lett.* **185**, 513–517.
28. Tredwell, C. J. and A. D. Osborne (1980) Viscosity dependent internal conversion in the rhodamine dye, fast acid violet 2R. *J. Chem. Soc. Farady Trans. 2* **76**, 1627–1637.
29. Lopez-Arbeola, F., I. Urrecha-Aguirresacona and I. Lopez-Arbeola (1989) Influence of the molecular structure and the nature of the solvent on the absorption and fluorescence characteristics of rhodamines. *Chem. Phys.* **130**, 371–378.
30. Lopez-Arbeola, I. and K. K. Rohatgi-Mukherjee (1986) Solvent effect on photophysics of the molecular forms of rhodamine B. Solvation models and spectroscopic parameters. *Chem. Phys. Lett.* **128**, 474–479; (1986) Solvent effects on the photophysics of the molecular forms of rhodamine B. Internal conversion mechanism. *Chem. Phys. Lett.* **129**, 607–614.
31. Kalyanasundaram, K. (1987) *Photochemistry in Microheterogeneous System.* Academic Press, New York.
32. Darmanyan, A. P. and C. S. Foote (1993) Solvent effects on singlet oxygen yield from n, π^* and π, π^* triplet carbonyl compounds. *J. Phys. Chem.* **97**, 5032–5035.
33. Darmanyan, A. P. (1993) Mechanism of singlet oxygen interaction with solvent removing prohibition of the radiative $^1\Delta_g \rightarrow {}^3\Sigma_g^-$ transition in oxygen. *Chem. Phys. Lett.* **215**, 477–482.
34. Rogers, M. A. (1983) Time resolved studies of 1.27 μm luminescence from singlet oxygen generated in homogeneous and microheterogeneous fluids. *Photochem. Photobiol.* **37**, 99–103.
35. Kessel, D. (1989) Exploring the multidrug resistance with rhodamine 123. *Cancer Commun.* **1**, 145–149.
36. Efferth, T., H. Lohrke and M. Volm (1989) Reciprocal correlation between expression of P-glycoprotein and accumulation of rhodamine 123 in human tumors. *Anticancer Res.* **9**, 1633–1638.